ACS Photonics

Letter

pubs.acs.org/journal/apchd5

Ultrasensitive Plasmonic Detection of Molecules with Graphene

Damon B. Farmer,*[,†] Phaedon Avouris,[†] Yilei Li,[‡,§] Tony F. Heinz,[‡,§] and Shu-Jen Han[†]

[†]IBM T. J. Watson Research Center, Yorktown Heights, New York 10598, United States

[‡]Department of Applied Physics, Stanford University, Stanford, California 94305, United States

[§]SLAC National Accelerator Laboratory, Menlo Park, California 94025, United States

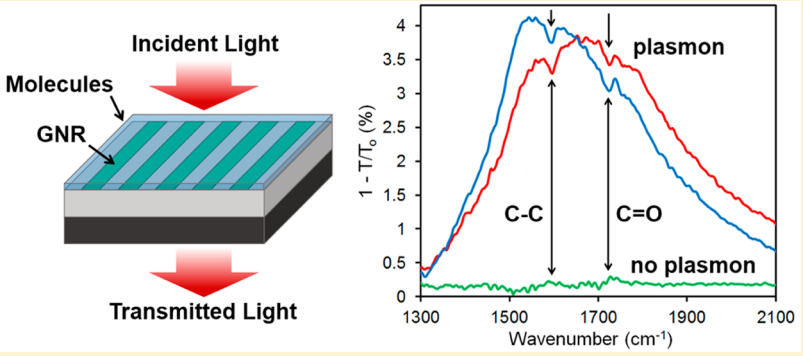

ABSTRACT: Graphene plasmons can couple with vibrations in both extended and local systems, for example, phonons in polar crystals and molecular vibrations in polymers. These interactions are characterized by plasmon-induced transparency features within the plasmon infrared absorption profile. Detection enhancement made possible by graphene-based plasmon-induced transparency has been demonstrated in both polymer and protein films and has shown to offer superior detection capabilities compared to conventional metal dipole plasmonic sensors. Here, we demonstrate the detection of molecular vibrations in minute, residual molecular quantities of solid- and gas-phase molecules down to 50 zeptomol/μm^2 using graphene plasmonic sensing platforms. Plasmon-induced transparency enhancement is shown to be sensitive to both the specific molecular coordination of the measured vibrations and to the distribution of modes within the measured vibrational bands. This work could lead to the development of functionalization-free, chemical-specific, large-area, signal-enhancement platforms for infrared spectroscopy.

KEYWORDS: *graphene, plasmon, molecules, sensing, detection, spectroscopy*

Plasmonic applications of graphene have recently been the subject of intense investigation for a variety of reasons.[1,2] As with conventional plasmonic materials, like silver and gold, the size and shape of graphene nano- and microstructures greatly influences their plasmonic properties.[3,4] In addition to this, and in contrast to metals, plasmonic properties in graphene can also be manipulated by modifying both the carrier concentration and the layering configuration of the structure.[3,5,6] By exploiting these characteristics within the parameter space of graphene plasmonics and considering the broadband light absorption afforded by graphene, plasmons with energies ranging from the mid-infrared (IR) to the far-infrared can readily be obtained. A high degree of subwavelength confinement of incident fields is exhibited in this spectral range, as is a short out-of-plane decay length of the plasmon field, giving graphene plasmons utility in both optical scaling and surface sensing.[7,8]

When graphene plasmons in the mid-IR couple with vibrations in molecules or phonons in polar crystals, plasmon-induced transparency (PIT) features can develop within the absorption profile of the plasmon resonance.[8−11] The detection enhancement made possible by this interaction has been demonstrated in relatively thick polymer and protein films, and has shown to offer superior detection capabilities compared to conventional metal dipole-antenna plasmonic sensors.[8,10] Here, we demonstrate the detection of vibrational modes in small quantities of solid-phase and gas-phase molecules using graphene plasmon sensing platforms with a commercial infrared spectrometer, and in doing so, demonstrate the potential of graphene as a functionalization-free, chemical-specific, molecular sensor.

Transferable graphene grown by chemical vapor deposition is used as the source material for the plasmonic structures, which are fabricated into nanoribbon arrays using conventional electron-beam lithography patterning and reactive ion etching techniques.[6,12] These nanoribbons are on a 280 nm thick layer of silicon dioxide, which is thermally grown on an IR-transparent silicon substrate (see Methods). A representative scanning electron microscope image of these nanribbon arrays is shown in Figure 1a, where arrays with nanoribbon widths of 90 to 150 nm are made. Nanoribbons are particularly good

Received: February 29, 2016
Published: April 7, 2016

DOI: 10.1021/acsphotonics.6b00143
ACS Photonics 2016, 3, 553−557

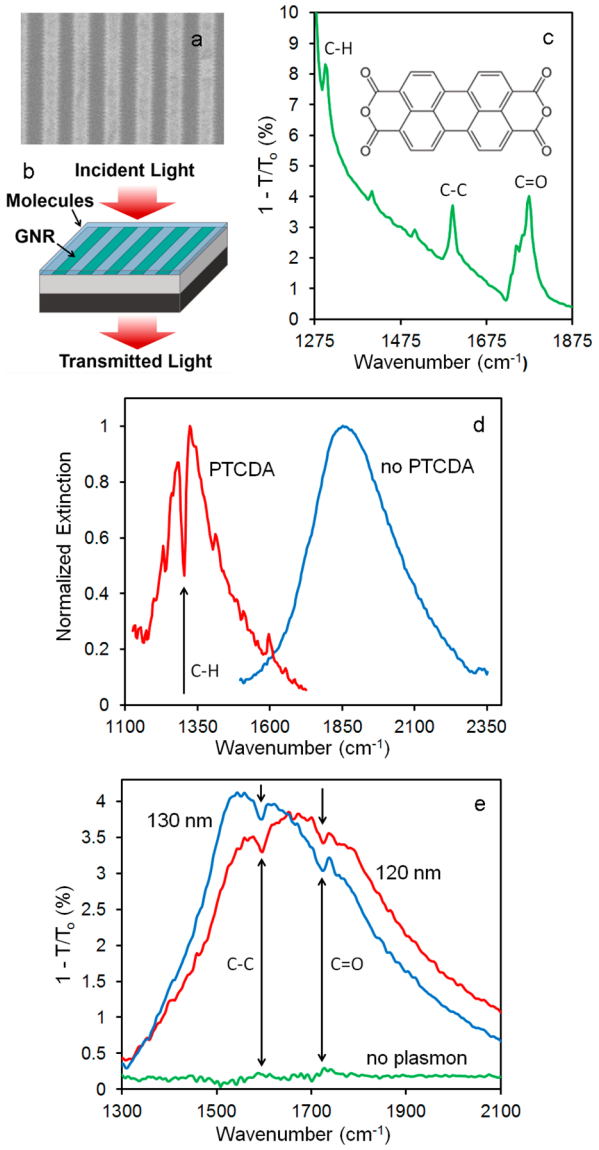

Figure 1. (a) SEM image of a graphene nanoribbon array. The widths of these nanoribbons are 120 nm. (b) Schematic of the measurement platform, with the graphene nanoribbons (GNR) on top of a SiO_2/Si substrate, and molecules deposited on top of the GNR array. (c) IR absorption spectrum of PTCDA, showing the positions of C−H bending modes, C−C ring breathing modes, and C═O stretching modes. The molecular structure of PTCDA is also shown. (d) Extinction spectra of graphene plasmon resonance with and without a 16 nm thick layer of PTCDA deposited onto the nanoribbon array surface. PIT caused by interaction with the C−H mode in PTCDA is shown. (e) Extinction spectra of two graphene plasmons (120 and 130 nm nanoribbon widths) with 0.6 nm of PTCDA deposited on the nanoribbon array surfaces. PIT caused by interaction with the C−C and C═O modes in PTCDA is evident within the resonance peaks. The extinction spectrum of 0.6 nm of PTCDA without the aid of the plasmon shows no definitive evidence of the C−C or C═O vibrations.

plasmonic structures to study because plasmons can be excited with incident radiation polarized perpendicular to, but not parallel to, the nanoribbon length. In this way, the plasmons can be turned "on" and "off", and effects arising from plasmonic excitation can be distinguished from other radiation absorption effects that may be present. Extinction spectra acquired by transmission Fourier transform infrared (FTIR) spectroscopy are used to analyze the resulting plasmonic activity of the samples, where plasmon excitation is characterized by an increase in light absorption at the plasmon resonance frequency. The ability to acquire spectroscopic information with transmitted light (Figure 1b) is a particularly advantageous property of graphene over opaque, metal plasmonic systems that are measured with a reflected, and consequently more lossy, light signal. Unless otherwise noted, extinction spectra are acquired using the transmission ratio T_{per}/T_{par}, where T_{per} and T_{par} are acquired using light polarized perpendicular and parallel to the nanoribbon length, respectively (see Methods).

Plasmon detection of perylene-3,4,9,10-tetracarboxylic dianhydride (PTCDA) is investigated first. This molecule has been extensively studied for its ability to form well-ordered, herringbone-type patterns on the graphene surface, a result of strong $\pi-\pi$ interactions between PTCDA and graphene.[13−15] It is a solid at room temperature and is deposited onto the nanoribbon arrays by thermal evaporation (see Methods). Infared absorption characteristics of PTCDA have been previously studied,[16,17] and assignment of selected vibrational absorption modes observed in the IR spectra are shown in Figure 1c. Thick films (16 nm) of PTCDA on nanoribbon arrays results in a redshift of the plasmon resonance frequency, which is due to the change in permittivity of the surrounding medium and the $\pi-\pi$ interactions previously discussed. By taking this shift into account, the plasmon resonance can be adjusted to overlap with a PTCDA vibrational mode, resulting in coupling and clear PIT behavior (Figure 1d).

When the PTCDA thickness is reduced to 0.6 nm, a thickness that is beyond the detection limit of the spectrometer alone, coupling with graphene plasmons allows for observation of PIT signatures associated with PTCDA vibrational modes. This is shown in Figure 1e, where adsorption peaks of two different plasmons are positioned so as to overlap with both C−C ring breathing modes around 1590 cm^{-1} and C═O stretching modes around 1730 cm^{-1}. Attempts to measure this thin PTCDA film in a region without the nanoribbon array reveals the inadequacy of the measurment system to detect the presence of these modes without the aid of the plasmon enhancement. With a molecular density of 1.28 g/cm^3 and mass of 392 g/mol for PTCDA, and considering that only 1/3 of the molecules contribute to the absorption due to randomness of the PTCDA orientation,[18] the amount of material on a nanoribbon array with 2000 μm^2 surface area is estimated to be 1 femtomole, which corresponds to 500 zeptomol/μm^2 (see Methods). Furthermore, the large signal-to-noise ratios present in the measurements suggests that detection of even smaller quantities should be possible.

Doping the nanoribbon arrays with nitrogen dioxide (NO_2), which is known to absorb strongly on and desorb slowly from graphene and other carbon surfaces,[19] allows for investigation of the PIT features as the plasmon resonance changes relative to the vibrational modes. The 0.6 nm PTCDA sample is exposed to pulses of NO_2 in a vacuum of 300 mTorr at 25 °C and then immediately measured in the FTIR spectrometer (see Methods). Doping from this gas causes a blueshift in the plasmon resonance due to an increase in free carrier concentration, as can be seen in Figure 2a. Slow desorption of NO_2 from the sample surface then causes this resonance to shift back toward its initial position over the course of several days, during which time the PIT of both the C−C and C═O vibrational modes can be studied. As expected, the induced transparency increases as the energy difference (ΔE) between the plasmon resonance and vibrational modes decreases

DOI: 10.1021/acsphotonics.6b00143
ACS Photonics 2016, 3, 553−557

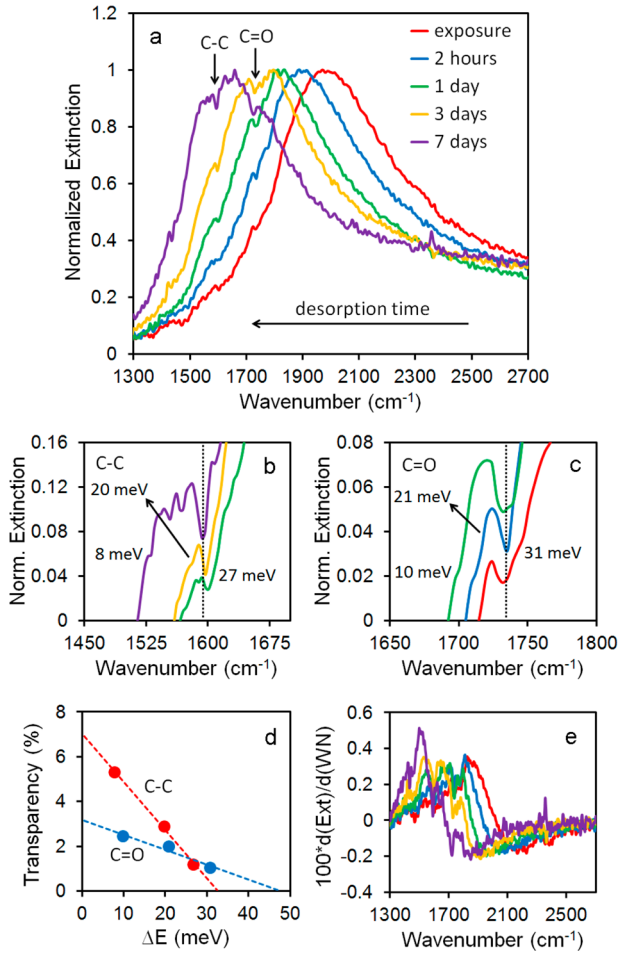

Figure 2. (a) Extinction spectra of a graphene plasmon with NO_2 exposure and subsequent desorption from the nanoribbon array surface. Detuning of the plasmon resonance with respect to the C−C and C═O vibrations in PTCDA changes with desorption time. (b, c) Higher resolution of the PIT behavior at different values of ΔE for both the C−C and C═O vibrations. The induced transparency is measured from the dip minimum to the crest maximum at the low energy side of the PIT feature. (d) Induced transparency vs detuning, as measured from (b) and (c), shows linear dependencies for both vibrations. (e) Corresponding derivatives of the plasmon absorption line shapes in (a), showing little variation other than shifting due to NO_2 desorption. The position of the C−C vibration is far from the spike in the t = 7 days curve (purple curve).

(Figure 2b,c). Further analysis reveals that the rate of this increase is different for the C−C modes and the C═O modes. As shown in Figure 2d, where the transparency is plotted with respect to the detuning ΔE, the resulting slope from the C−C modes is more than a factor of 2 greater than that of the C═O modes. Extrapolating to ΔE = 0, where the vibrations are in exact resonance with the plasmon frequency, gives 3.2% transparency for the C═O interaction and 7% transparency for the C−C interaction. Hence, the plasmon interaction with C−C is comparatively stronger. These plasmon−vibrational mode interactions are in contrast to the photon−vibrational mode interactions, where the C═O modes absorb more light than the C−C modes (Figure 1c). This discrepancy is likely due to the π−π interaction between PTCDA and graphene, which enhances the coupling between the plasmon and the C−C breathing modes, but not the C═O stretching modes.

The depth of the induced transparency depends on several parameters and can be modeled and understood in the context of coupled oscillators, where only one of the oscillators is driven by an external force.[20,21] These dynamics are described by the equations:

$$\ddot{x}_A(t) + \gamma_A \dot{x}_A(t) + \omega_A^2 x_A(t) + \kappa x_P(t) = F(t) \quad (1)$$

$$\ddot{x}_P(t) + \gamma_P \dot{x}_P(t) + \omega_P^2 x_P(t) + \kappa x_A(t) = 0 \quad (2)$$

where $F(t)$ is the external force that drives the active oscillator with position x_A, resonance frequency ω_A, and damping γ_A. This oscillator is coupled to a passive oscillator with corresponding parameters x_P, ω_P, and γ_P through the coupling function κ. Solving these coupled differential equations yields the power dissipation of the system, which is analogous to the experimentally measured absorption spectra.[20,21] Within this framework, the transparency depth is influenced by the coupling between oscillators, the detuning $\Delta E = \hbar|(\omega_A - \omega_P)|$, and the damping experienced by the oscillators. Increasing the coupling leads to increased transparency, while increasing both the detuning and damping leads to decreased transparency (Figure 3a).

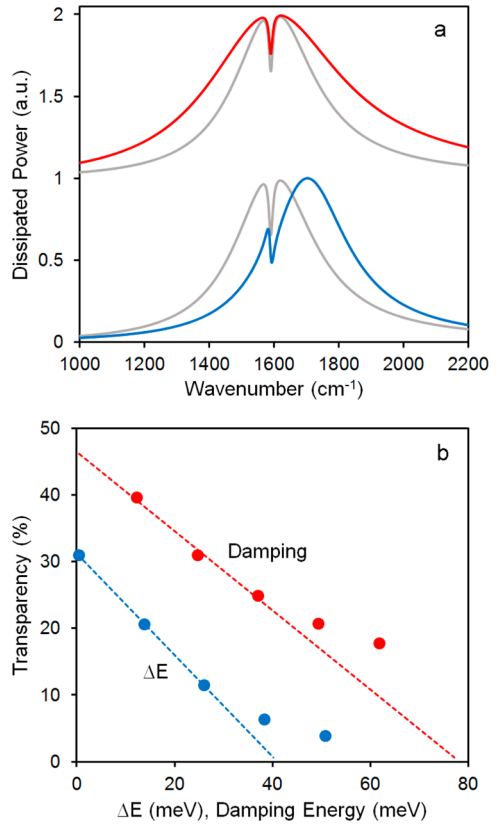

Figure 3. (a) Representative results of the coupled oscillator model, showing the effects of damping and detuning on the magnitude of PIT. Here, the dissipated power of the system is found as outlined in refs 20 and 21. With a coupling constant of 0.26 and ω_P = 1590 cm^{-1} for all curves, the reference curves (gray curves) have parameters γ_A = 37.2 meV and ΔE = 0.56 meV, while ΔE = 14 meV for the blue curve and γ_A = 62 meV for the red curve. (b) Corresponding plots of damping and detuning at more energies, also determined using the coupled oscillator model, shows roughly linear behavior at small energies. The dashed lines serve as guides showing the deviation from linear behavior at higher energies.

DOI: 10.1021/acsphotonics.6b00143
ACS Photonics 2016, 3, 553−557

In the plasmon-vibrational mode system, the graphene plasmon is the strongly absorbing active mode that is driven by the external IR field, and the more weakly absorbing molecular vibration is the passive (dark) mode that is coupled to the plasmon. The linear dependence of the transparency on detuning experimentally observed in Figure 2d is reflected in the coupled oscillator model for small ΔE values (Figure 3b) and also agrees with observations obtained using conventional metal plasmonic systems.[22] Nonlinearity seen in the model cannot be measured in the experiment because of signal-to-noise limitations as ΔE increases. Since damping experienced by graphene plasmons can increase at higher resonance energies, where more damping pathways become available, it is also necessary to investigate the extent to which changes in plasmon damping contributes to the induced transparencies shown in Figure 2. As the plasmon resonance frequency decreases with NO_2 desorption, the overall line shape of the plasmon absorption, particularly in the vicinities of the C−C and C═O vibrations, does not significantly change. This is seen by comparing the instantaneous slopes (first derivatives) of the absorption line shapes (Figure 2e). From this, it can be concluded that effects of relative damping changes on the measured transparencies are minimal and that it is detuning that is predominantly responsible for the induced transparency changes observed in Figure 2d. The C−C absorption band, which spans approximately 6 meV, is composed of two stretching modes, while the broader C═O band, which spans approximately 12 meV, is composed of four stretching modes (Figure 1c).[16] If all of these optically accessible modes can also couple to the plasmon, then this may explain the smaller rate of change of the C═O induced transparency observed in Figure 2d. Here, the broader spread of the C═O modes causes the transparency to decay at a slower rate than the C−C modes as the detuning increases, resulting in the smaller slope observed for C═O.

Previous work on graphene plasmonic sensing has dealt only with the detection of solid-phase materials. Figure 4 shows the PIT-facilitated detection of C═O and C−C vibrations in acetone and hexane vapor. These vapors are delivered using nitrogen carrier gas flowing at 80 sccm that is circulated into vapor containment vessels and exhausted through a nozzle positioned 1 cm from the nanoribbon array surface. Though the residence of these molecules on or near the graphene surface is transient, it is clear from these spectra that the plasmon and vibrational modes of molecules within the detection volume above the nanoribbon array surface indeed interact to produce PIT behavior. The samples are not enclosed, so the vapor/nitrogen mixture is dispersed into the atmosphere. However, an upper limit of the vapor concentrations within the plasmon sensing volume can be made based on the respective temperature dependent partial pressures of the vapors. With an out-of-plane field decay length of 20 nm for graphene plasmons,[8,10] estimated concentrations on the order of 0.1 femtomoles (50 zeptomol/μm^2) are obtained for both molecules (see Methods).

Utilization of graphene plasmonic structures as signal enhancement platforms, onto which residual amounts of material can be deposited and detected, is a potentially very useful technique that is straightforward to integrate into current commercial IR spectroscopy technology. Further investigation into this burgeoning field will allow us to better determine its full potential. Better graphene nanoribbon material quality will allow for less plasmon damping, and hence, improved detection

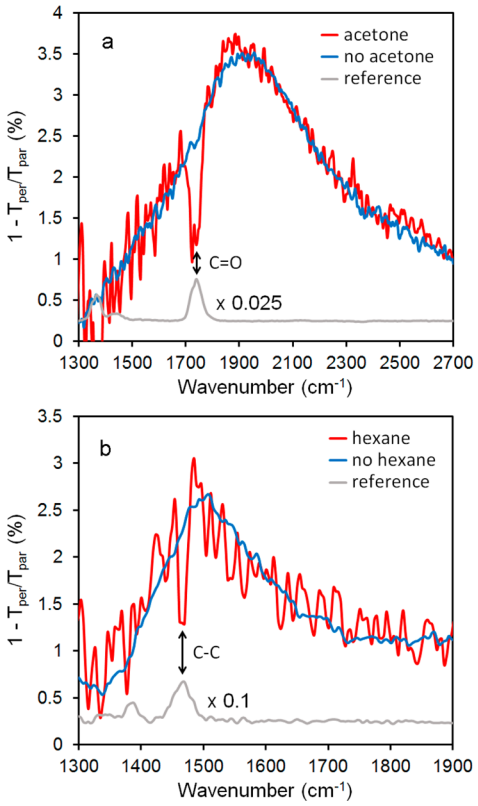

Figure 4. Extinction spectra showing PIT behavior in graphene plasmon absorption when exposed to vapor-phase molecules. (a) C═O vibrational modes in acetone and (b) C−C vibrational modes in hexane are readily detected. The spectra of bulk vapors are also included as reference (gray curves). Noise in the absorption spectra occurs due to fluctuations in the local refractive index as the vapor flows over the sample.

sensitivity and resolution. Also, proper functionalization could be incorporated to enhance the chemical selectivity of this sensor or be used to preferentially position molecules over areas of the nanoribbons where the plasmon field is strongest, thus boosting the field enhancement.

METHODS

Graphene on copper foil is acquired from Graphene Industries. Poly(methyl methacrylate) (A3 PMMA) obtained from MicroChem is spun onto the topside of this foil at 3000 rpm for 60 s. The foil is then placed so as to float on top of a copper etchant (Transene CE-200), where the backside of the foil makes contact with the etchant. After 1 min, the backside is rinsed with water and then returned to the etchant, where it is allowed to float until the copper is totally dissolved. The remaining PMMA/graphene film is scooped onto a silicon wafer and repeatedly transferred to water baths until the etchant is appreciably diluted. This film is then transferred to the IR-transparent substrate and blow-dried with nitrogen. The PMMA layer is removed in acetone at 70 °C, and the substrate is rinsed with isopropanol and blow-dried with nitrogen. PMMA is then spun onto the substrate as before and baked on a hot plate at 175 °C for 5 min, after which electron-beam lithography and pattern development is used to define the nanoribbon array pattern. Oxygen reactive-ion etching is then used to remove the exposed graphene regions (50 W, 20 sccm O_2, 30 mTorr, 30 s), and the PMMA is subsequently removed

DOI: 10.1021/acsphotonics.6b00143
ACS Photonics 2016, 3, 553−557

in acetone at 25 °C and allowed to dry in air, completing the sample fabrication procedure.

A Thermo Fisher Nicolet 8700 FTIR spectrometer with a Continuum IR microscope is used as the measurement apparatus. Spectra of plasmon absorption and molecular absorption are acquired by first taking a background spectrum of the substrate. This background is either the substrate with an absence of PTCDA or graphene plasmon excitation (T_o) or the substrate with the nanoribbon array using parallel polarized light (T_{par}). Spectra with PTCDA, graphene plasmon excitation, acetone, or hexane are then taken to determine T or T_{per}, allowing for the transmission ratios T/T_o and T_{per}/T_{par} to be found. Some extinction spectra are normalized in order to compare the percentage of induced transparency relative to the total plasmon absorption.

PTCDA is thermally deposited onto the sample surface following similar procedures outlined in ref 13. A quartz crystal microbalance is used as feedback to control the depositon rate and thickness, and the thickness is confirmed and calibrated using atomic force microscopy. The concentration (C) of PTCDA is calculated using the procedure outlined in ref 18, using the formula $C = thwD/3M$, where t is the PTCDA thickness, hw is the detection area (total nanoribbon array area), D is the molecular density, and M is the molecular mass.

Nitrogen dioxide doping is carried out in an atomic layer deposition system. At 25 °C under a vacuum pressure of 300 mTorr in flowing argon, 50 cycles of 5 mL doses of NO_2 are dosed over the sample. The sample is then removed and immediately measured in the FTIR spectrometer. With slow NO_2 desorption, subsequent measurments are then made over the next several days. Acetone and hexane vapors are flowed over the sample surface through a nozzle that is positioned 1 cm from the sample. These vapors are delivered with a nitrogen carrier gas, which flows at 80 sccm through a 250 mL bubbler that is half-filled with these volatile solvents. The solvent temperature is measured to be 5 °C for both acetone and hexane during this process. Partial pressures of these solvents are calculated at this temperature using the Antoine equation and are found to be 90 Torr for acetone and 59 Torr for hexane, which are then used to determine an upper estimate of the molecular concentrations within the detection volume of the plasmons using the ideal gas law.

AUTHOR INFORMATION

Corresponding Author

*E-mail: dfarmer@us.ibm.com.

Notes

The authors declare no competing financial interest.

ACKNOWLEDGMENTS

The authors are grateful to J. Bucchignano and S. Dawes for expert technical assistance involving electron-beam lithography.

REFERENCES

(1) Grigorenko, A. N.; Polini, M.; Novoselov, K. S. Graphene Plasmonics. *Nat. Photonics* **2012**, *6*, 749−758.

(2) Low, T.; Avouris, P. Graphene Plasmonics for Terahertz to Mid-Infrared Applications. *ACS Nano* **2014**, *8*, 1086−1101.

(3) Ju, L.; Geng, B.; Horng, J.; Girit, C.; Martin, M.; Hao, Z.; Bechtel, H. A.; Liang, X.; Zettl, A.; Ron Shen, Y.; Wang, F. Graphene Plasmonics for Tunable Terahertz Metamaterials. *Nat. Nanotechnol.* **2011**, *6*, 630−634.

(4) Yan, H.; Low, T.; Zhu, W.; Wu, Y.; Freitag, M.; Li, X.; Guinea, F.; Avouris, P.; Xia, F. Damping Pathways of Mid-Infrared Plasmons in Graphene Nanostructures. *Nat. Photonics* **2013**, *7*, 394−399.

(5) Yan, H.; Li, X.; Chandra, B.; Tulevski, G.; Wu, Y.; Freitag, M.; Zhu, W.; Avouris, P.; Xia, F. Tunable Infrared Plasmonic Devices Using Graphene/Insulator Stacks. *Nat. Nanotechnol.* **2012**, *7*, 330−334.

(6) Farmer, D. B.; Rodrigo, D.; Low, T.; Avouris, P. Plasmon-Plasmon Hybridization and Bandwidth Enhancement in Nanostructured Graphene. *Nano Lett.* **2015**, *15*, 2582−2587.

(7) Koppens, F. H. L.; Chang, D. E.; Abajo, J. G. Graphene Plasmonics: A Platform for Strong Light-Matter Interactions. *Nano Lett.* **2011**, *11*, 3370−3377.

(8) Li, Y.; Yan, H.; Farmer, D. B.; Meng, X.; Zhu, W.; Osgood, R. M.; Heinz, T. F.; Avouris, P. Graphene Plasmon Enhanced Vibrational Sensing of Surface-Absorbed Layers. *Nano Lett.* **2014**, *14*, 1573−1577.

(9) Yan, H.; Low, T.; Guinea, F.; Xia, F.; Avouris, P. Tunable Phonon-Induced Transparency in Bilayer Graphene. *Nano Lett.* **2014**, *14*, 4581−4586.

(10) Rodrigo, D.; Limaj, O.; Janner, D.; Etezadi, D.; Abajo, F. J. G.; Pruneri, V.; Altug, H. Mid-Infrared Plasmonic Biosensing with Graphene. *Science* **2015**, *349*, 165−168.

(11) Jia, Y.; Zhao, H.; Guo, Q.; Wang, X.; Wang, H.; Xia, F. Tunable Plasmon-Phonon Polaritons in Layered Graphene-Hexagonal Boron Nitride Heterostructures. *ACS Photonics* **2015**, *2*, 907−912.

(12) Li, X.; Cai, W.; An, J.; Kim, S.; Nah, J.; Yang, D.; Piner, R.; Velamakanni, A.; Jung, I.; Tutuc, E.; Banerjee, S. K.; Colombo, L.; Ruoff, R. S. Large-Area Synthesis of High-Quality and Uniform Graphene Films on Copper Foils. *Science* **2009**, *324*, 1312−1314.

(13) Wang, Q. H.; Hersam, M. C. Room-Temperature Molecular-Resolution Characterization of Self-Assembled Organic Monolayers on Epitaxial Graphene. *Nat. Chem.* **2009**, *1*, 206−211.

(14) Huang, H.; Chen, S.; Gao, X.; Chen, W.; Thye Shen Wee, A. Structural and Electronic Properties of PTCDA Thin Films on Epitaxial Graphene. *ACS Nano* **2009**, *3*, 3431−3436.

(15) Tian, X. Q.; Xu, J. B.; Wang, X. M. Self-Assembly of PTCDA Ultrathin Films on Graphene: Structural Phase Transition and Charge Transfer Saturation. *J. Phys. Chem. C* **2010**, *114*, 20917−20924.

(16) Akers, K.; Aroca, R.; Hor, A. M.; Loutfy, R. O. Molecular Organization in Perylenetetracarboxylic Dianhydride Films. *J. Phys. Chem.* **1987**, *91*, 2954−2959.

(17) Scholz, R.; Friedrich, M.; Salvan, G.; Kampen, T. U.; Zahn, D. R. T.; Frauenheim, T. Infrared Spectroscopic Study of the Morphology of 3,4,9,10-Perylene Tetracarboxylic Dianhydride Films Grown on H-Passivated Si(111). *J. Phys.: Condens. Matter* **2003**, *15*, S2647−S2663.

(18) Adato, R.; Yanik, A. A.; Amsden, J. J.; Kaplan, D. L.; Omenetto, F. G.; Hong, M. K.; Erramilli, S.; Altug, H. Ultra-Sensitive Vibrational Spectroscopy of Protein Monolayers with Plasmonic Nanoantenna Arrays. *Proc. Natl. Acad. Sci. U. S. A.* **2009**, *106*, 19227−19232.

(19) Kong, J.; Franklin, N. R.; Zhou, C.; Chapline, M. G.; Peng, S.; Cho, K.; Dai, H. Nanotube Molecular Wires as Chemical Sensors. *Science* **2000**, *287*, 622−625.

(20) Taubert, R.; Hentschel, M.; Kastel, J.; Giessen, H. Classical Analog of Electromagnetically Induced Absorption in Plasmonics. *Nano Lett.* **2012**, *12*, 1367−1371.

(21) Taubert, R.; Hentschel, M.; Geissen, H. Plasmonic Analog of Electromagnetically Induced Absorption: Simulations, Experiments, and Coupled Oscillator Analysis. *J. Opt. Soc. Am. B* **2013**, *30*, 3123−3134.

(22) Vogt, J.; Huck, C.; Neubrech, F.; Toma, A.; Gerbert, D.; Pucci, A. Impact of the Plasmonic Near- and Far-Field Resonance-Energy Shift on the Enhancement of Infrared Vibrational Signals. *Phys. Chem. Chem. Phys.* **2015**, *17*, 21169−21175.

DOI: 10.1021/acsphotonics.6b00143
ACS Photonics 2016, 3, 553−557